Photothermal Polarimetric Nanoscopy: An Emerging Technique for Fingerprinting Minerals of Extraterrestrial Origin

T. Shay, K. Hinrichs,* S.G. Pavlov, N. Stojanovic, I. Weber, A. Morlok, and M. Gensch*



Cite This: ACS Earth Space Chem. 2025, 9, 2388-2394

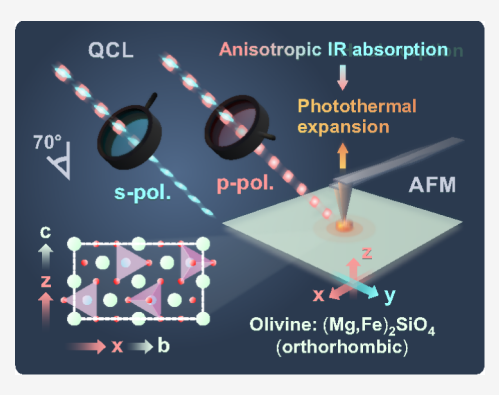


ACCESS I

Metrics & More

Article Recommendations

ABSTRACT: Nanospectroscopic investigations of the mineralogical composition of materials returned via sample-return missions are crucial for our understanding of the origin and evolution of planetary objects in our Solar System. Here, we show that the emerging technique of photothermal polarimetric nanoscopy, a variant of atomic force microscopy-based infrared spectroscopy, enables one to derive infrared fingerprint spectra of minerals noninvasively on the nanoscale. Besides the spatially resolved identification of specific minerals and mineral phases, the evaluation of the polarization dependence of the photoinduced nanomechanical response, in combination with optical reference data, may allow the deduction of valuable structural information on individual nanocrystallites or grains embedded in solid matrices.



KEYWORDS: infrared spectroscopy, nanoscopy, planetary materials, minerals, optical anisotropy

INTRODUCTION

Downloaded via DLR BIBLIO INFORMATIONSWESEN on October 17, 2025 at 07:38:06 (UTC). See https://pubs.acs.org/sharingguidelines for options on how to legitimately share published articles

Studying minerals of extraterrestrial origin has been an important approach to unravel the geochemistry and, thereby, the origin and evolution of planetary bodies in our Solar System for more than two centuries. The first investigations of this type focused on the mineralogy of meteorites as early as the beginning of the 19th century and have since identified the presence of more than 250 different mineral species, reflecting diverse environments and formation conditions.² Optical spectroscopy, in particular vibrational spectroscopy techniques such as infrared spectroscopy or Raman spectroscopy, has played an important role since its emergence as an established research tool in the mid-20th century. Spectroscopy in the long-wavelength range, from the infrared to the THz range, has been employed successfully for the investigation of planets, moons, asteroids, or interstellar matter via remote sensing (see, e.g., 3-5) and, already very early on, for studying material returned from the Moon. Sample return missions are becoming increasingly feasible and have, in the meantime, successfully returned samples from beyond Earth's orbit providing material from the solar wind, the comet Wild 2,8 and the asteroids Itokawa⁹ and Ryugu.¹⁰ Optical techniques, in particular those sensitive to the vibrational fingerprint, which enable noninvasive access to structural and compositional properties beyond what can be derived from remote sensing or robotic explorations, are therefore in very high demand. Because of the heterogeneous nature of many planetary materials, Raman or infrared microspectroscopy has frequently been employed (see, e.g., refs ^{10,11}), and there are some examples of employing nanospectroscopy techniques such as infrared scattering near-field optical microscopy (IR-SNOM)¹² and atomic force microscopy-based infrared spectroscopy (AFM-IR). 13-16

Surface planetary materials are often fine-grained. They form heterogeneous superficial deposits, often referred to as regolith, which are typically affected by strong physical and chemical weathering processes¹¹ and are commonly dominated by submicron grains. Small grains embedded in large solid matrices can hold crucial information about the origin and age of celestial bodies. Mesoscale data on the inclusion structure, e.g., measured as mean grain orientation, can be used for placing constraints on metamorphic history or impactors, for example, in the characterization of chondritic meteorites. For fine regolith particles, such as those returned by the space missions to near-Earth asteroids, the accurate combined microstructural and chemical resolution of individual microcraters and inclusions (with typical sizes <1 μ m) has revealed important insights into the the interaction of solar system asteroids with interplanetary dust.13

The aim of this study is to investigate whether polarizationresolved AFM-IR or photothermal polarimetric nanoscopy

Received: April 28, 2025 Revised: July 23, 2025 Accepted: September 3, 2025 Published: September 11, 2025





(PPN), respectively, is a suitable approach to study the structure and composition of minerals on the nanoscale and, hence, can represent a complementary technique to infrared and Raman microspectroscopies in planetary and Earth sciences.

In the AFM-IR method, the AFM tip probes the local photothermal expansion of a sample upon laser radiation. The spatial resolution of AFM-IR significantly surpasses the diffraction-limited lateral resolution of classical far-field optical experiments. Typical lateral resolutions are in the range of about 10–30 nm and depend on a complex interplay of parameters, such as the measurement mode, the probing depth, the laser pulse rates, thermal conductivity, and interfacial thermal resistance. ^{19–21} The method is an "indepth probing technique" which can probe depths of a few hundred nanometers ^{21,22} to a few micrometers at frequencies with low absorption. ²² By adapting pulsing parameters, the surface selectivity can be improved. ²³

Adding a polarization control allows probing anisotropic absorption of organic and inorganic samples at the nanoscale. Dazzi et al. showed that the measured AFM-IR signal relates to the sample absorbance in cases where the variation of the refractive index is small and, in general, relates to the imaginary part of the dielectric function. In AFM-IR measurements, the anisotropic absorption properties of thin films or bulk materials are caused by the anisotropic dielectric function and, e.g., preferential directions of transition dipole moments along defined axes. However, for thin films and structured surfaces, anisotropic absorption can also be induced by anisotropic contributions of field intensities.

Different olivine samples with varying levels of complexity are studied. Analytical challenges include the varying sizes of anisotropic crystalline olivine inclusions (ranging from nanometers to micrometers) within a surrounding matrix. To show the principle's applicability, a natural olivine single crystal is studied first. Afterward, the method is applied to the investigation of olivine samples with increasing complexity, olivine nanograins in a multicrystalline sample and a few 10 μ m-sized inclusions in a glass matrix.

■ EXPERIMENTAL SECTION

Olivine is a common mineral phase in all rocky planetary environments. Furthermore, planetary materials tend to be very fine-grained on submicron scales. Therefore, olivine in matrices serves as an ideal starting point. ²⁶

Olivine Samples. Two natural olivine samples, provided by the Institute for Geosciences at the University of Jena (Germany), were investigated in this work.²⁷

The homogeneous forsterite (Fo90.5) single crystal, with a polished surface and the c-axis oriented normal to it (parallel to z), was aligned with the plane of incidence (xz-plane in all experiments) so that the a- and b-axes were parallel to y and x, respectively, see Figure 1. The multicrystalline sample with slightly different forsterite content (Fo91.3), included differently oriented crystalline domains.²⁷

Both samples were regularly cut and polished using lapidary techniques to prepare minerals for optical studies.

In detail, the samples were embedded in epoxy resin, and the block was cut with a diamond saw. The selected halves were fixed on a sample holder on a specialized lapping/polishing machine to ensure homogeneous polishing and an entirely flat and planar surface without any curvature.

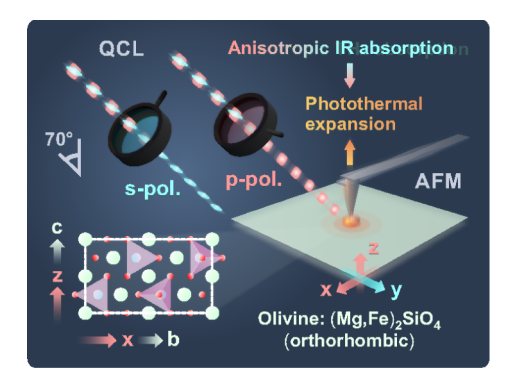


Figure 1. Fundamental principle of photothermal polarimetric nanoscopy (PPN) and experimental geometry in the study of the single-crystal olivine sample. PPN is based on the evaluation of the polarization of atomic force microscopy-based infrared spectroscopy (AFM-IR).

The sample surface was polished using progressively finer abrasives (diamond paste in suspension) on a polishing cloth to ensure optical quality, with the final grain size of 0.25 μ m.

Experimental Setup. The PPN measurements²⁴ were performed using a commercial AFM-IR platform (nanoIR2-FS, Anasys Instruments/BRUKER) equipped with an external cavity quantum cascade laser (QCL) (MIRcat, Daylight Solutions) in a top down geometry. The setup was mounted on a vibration isolation table. Experiments were conducted under ambient conditions, i.e., at room temperature and a stable humidity level below 2%, controlled by dry air purging. Measurements were performed in contact mode using goldcoated silicon AFM tips (0.07–0.4 N/m spring constant) with a nominal radius of curvature of the tip apex ≈30 nm, serving as a benchmark for the lateral resolution of the AFM-IR method. 13 Switching the polarization state (p- to s-polarized and vice versa) of the intrinsically linearly polarized QCL pulses (100:1 extinction ratio) was achieved by implementing an automated polarization rotator consisting of a series of flat Au mirrors. QCL light with a spectral range of 900–1125 cm⁻¹ and an average power of less than 0.45 mW (olivine single crystal), 0.91 mW (nanocrystallite), and 0.1 mW (microcrystallite) was focused under the tip with a spot size of about $50 \ \mu m \times 17 \ \mu m$ at an angle of incidence to the surface normal of 70°. For the chosen settings, a local temperature rise of a few K is possible; about 6 K was expected in a study of silica glasses in the center of the IR beam (2 mW, 100 s pulse width).²² For such temperature rises in the range of a few K, damage to the studied samples is not expected.

The tunable QCL pulse rate was synchronized with one-third (197 kHz for the olivine single crystal, 224 kHz for nanocrystallite, and 134 kHz for the microcrystallite) of the low-noise fourth bending mode of the AFM cantilever in contact with the sample. The resonant cantilever oscillation signal, collected by the AFM deflection detection system, was filtered using a bandpass filter with a window of 50 kHz around the central frequencies (591, 672, and 403 kHz, respectively). The photothermal expansion measurements were normalized to the corresponding polarization-dependent QCL background collected by the IR detector before focusing on the sample. The mechanical resonance enhancement of the cantilever oscillation amplitude allows for high sensitivity of the method, down to ultrathin films and monolayers. ^{28–30} A spectral resolution of 1 cm⁻¹ was accessible at a 20 cm⁻¹/s QCL sweep

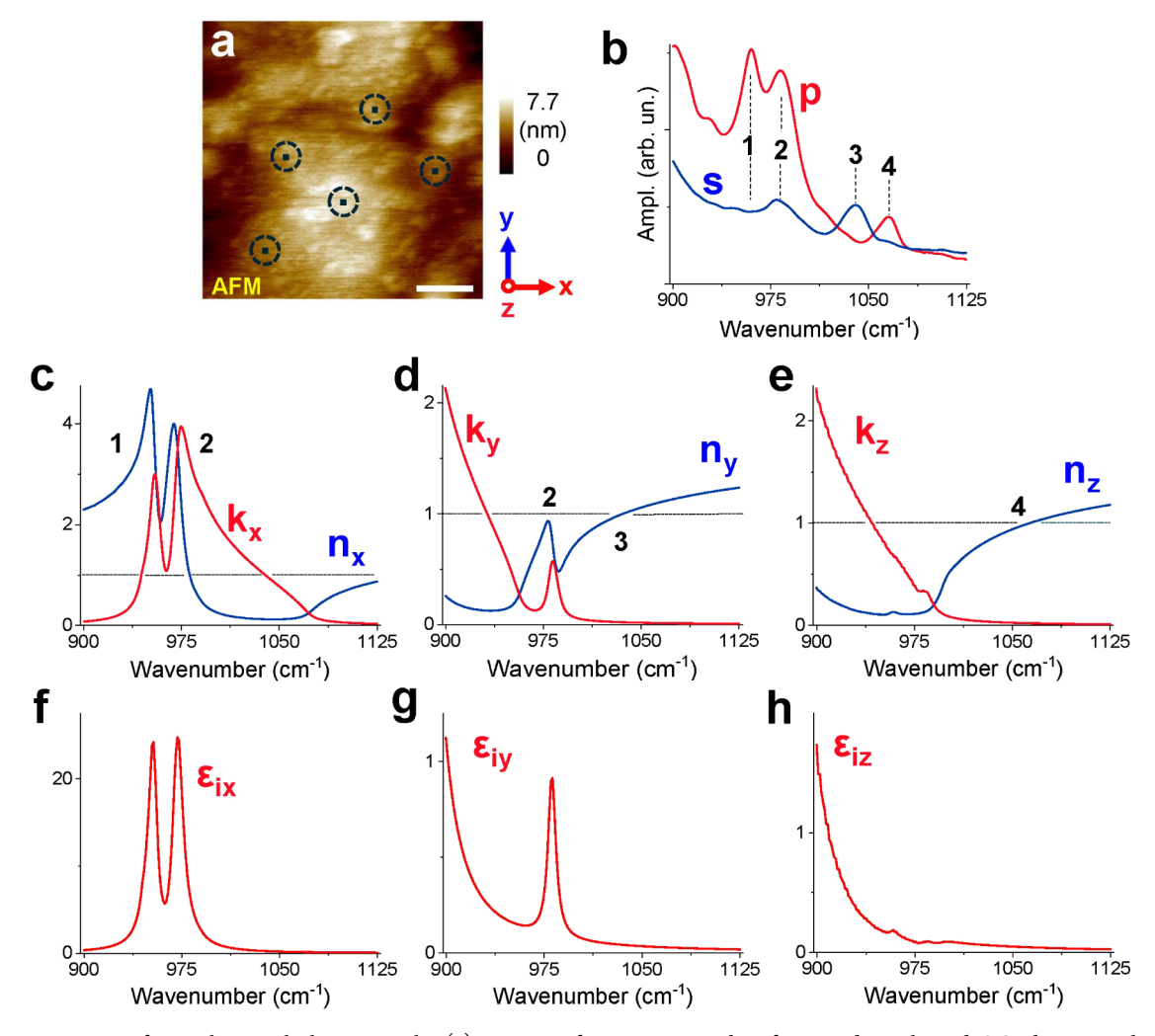


Figure 2. AFM image of a single-crystal olivine sample: (a) Average of PPN spectra taken for s- and p-polarized QCL beams at the indicated positions. Scale bar is 200 nm (b) and anisotropic optical constants as taken from ref 31 (c-e). On bottom the respective imaginary parts of epsilon are shown (f-h). Reference n and k data of a natural olivine single crystal (Mg1.9Fe0.1SiO4) along the b-, a-, and c-axes correspond to the indicated x-, y-, and z-axes of the sample, respectively. Adapted with permission from ref. 31. Copyright 2001 EDP Sciences.

rate, corresponding to an an acquisition time of 11.3 s per spectrum, currently limited by the external cavity grating stabilization time of the QCL. Savitzky—Golay filtering (third order, five points) was applied to the spectral data. AFM height images (500×300 pixels) were measured using a scan rate of 0.40, 0.25, and 0.2 Hz per line (for olivine single crystal, nanocrystallite, and microcrystallite, respectively). The acquisition time for single-wavenumber photothermal expansion images of olivine nanocrystallite was therefore 20 min per image, currently limited by the AFM scan rate. Only the data in the retrace scan direction were collected, i.e., the stage moving in the x-direction toward the laser source (see Figure 1). The images were flattened (first order) using the built-in nanoIR2-FS software, Anasys Studio 3.12.

RESULTS

Olivine Single Crystal. Figure 2 shows, at the top, an AFM image as well as averaged s- and p-polarized PPN spectra of a natural olivine single crystal ($Mg_{1.9}Fe_{0.1}SiO_4$) sample. The probed measurement spots are marked. Bands in the PPN spectra are related to the anisotropic SiO_4 stretching vibrations (peak 1 at about 960 cm⁻¹; peak 2 at about 983 cm⁻¹) and to

the Christiansen feature (n = 1 effects, see peak 3 at about 1040 cm⁻¹ and peak 4 at about 1065 cm⁻¹).

In the measurement geometry used at a 70° incidence angle, the p-polarized radiation has field components in x- and zdirections of the sample (Figure 1), and therefore, the measured p-polarized photothermal signal is proportional to the sum of the imaginary parts of the dielectric function in these directions. In contrast, the s-polarized radiation only has field components in the y-direction of the sample and, therefore, can only be related to the imaginary part of the dielectric function in y-direction. From the comparison with literature reference data³¹ of the direction-dependent optical constants (n, k) in Figure 4c-e, we confirm that the x, y, z-axes of the olivine single crystal sample are parallel to the crystallographic b-, a-, and c-axes, respectively. In particular, the bands observed in the measured s-polarized spectrum in Figure 2b can only be related to the olivine single crystal optical constants in the y-direction (a-axis).

The measurements of the single crystal exemplarily show that, similar to the analysis of organic films, conventional AFM-IR enables fingerprinting and that PPN, furthermore, can provide access to information about the orientation of the investigated crystals.

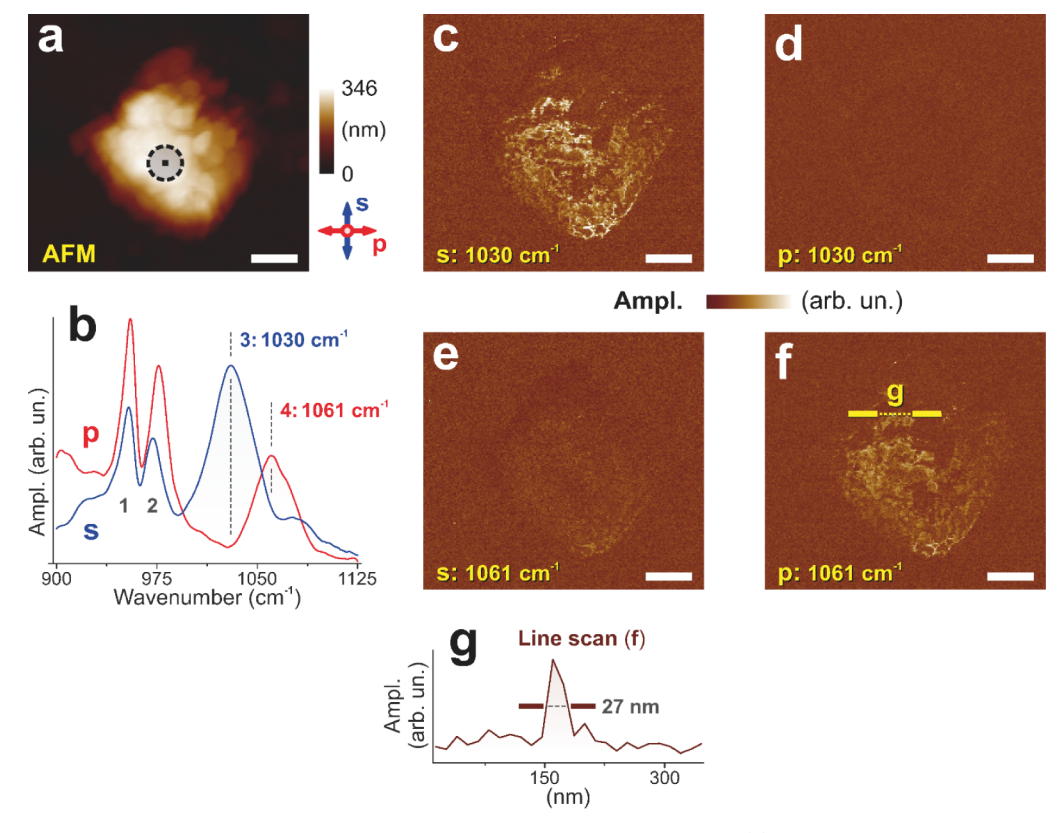


Figure 3. PPN measurements of a multicrystalline olivine sample. Scale bars are 500 nm. (a) AFM image with marked points selected for polarization-dependent spectra acquisition. (b) s- and p-polarized PPN spectra. (c-f) s- and p-polarized PPN maps at the frequencies of peaks 3 and 4 of the nanocrystallite (left to right and top to bottom, respectively). (g) Demonstrates the 27 nm lateral resolution of the method.

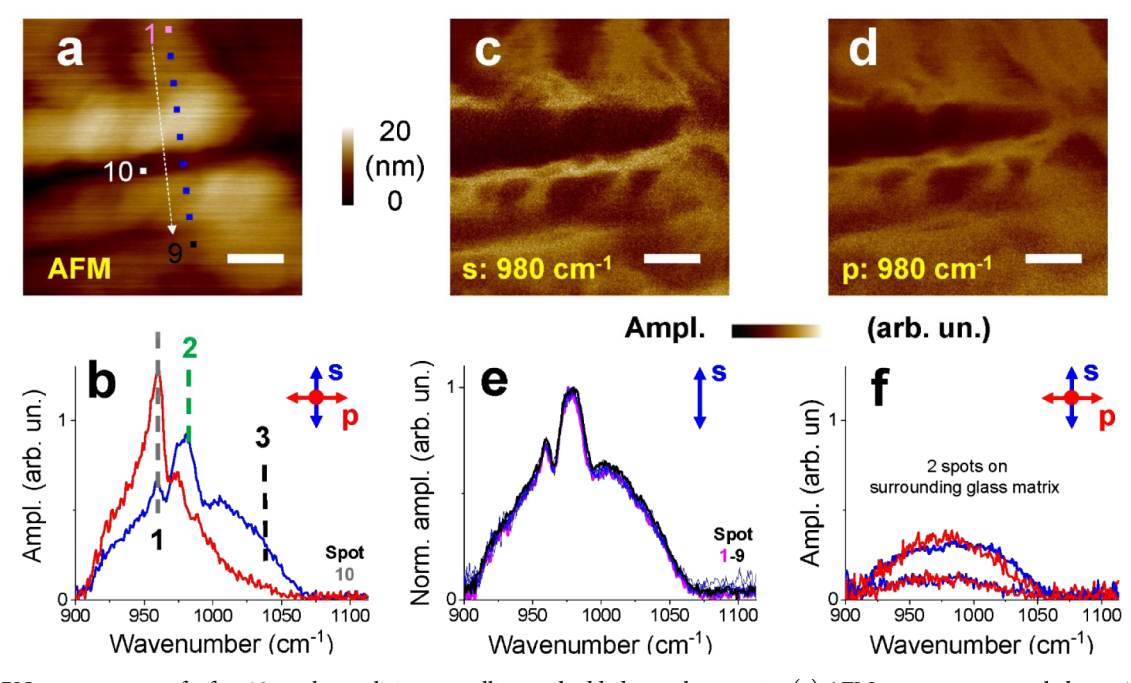


Figure 4. PPN measurement of a few 10 μ m large olivine crystallites embedded in a glass matrix. (a) AFM measurement; scale bar = 100 nm. The 10 spots measured by PPN are indicated. (b) s- and p-polarized PPN spectra at position 10. (e) Normalized s-polarized PPN spectra along one line from positions 1 to 9. (c, d) PPN maps of the sample at the frequency of peak 2 (980 cm⁻¹) and (f) two exemplarly s- and p-polarized PPN spectra at two positions on the surrounding amorphous glass matrix (outside of the range of the AFM images).

Nanograin in Multicrystalline Olivine. Figure 3a displays an AFM image of a multicrystalline olivine sample. A point marks the spot that was selected for the subsequent PPN spectra and image acquisition. Peaks 3 and 4 associated

with the Christiansen effect (n = 1 of the a- and c-crystal axes), appear in either the s- or p-polarized spectrum in a similar order as for the single crystal (Figure 2b). However, unlike the single crystal, peaks 1 and 2 are observed for both the s- and p-

Table 1. Comparison of Nanospectroscopic Techniques Previously Employed to Study Mineral Samples

Technique	Infrared- active	Raman- active	Spatial resolution	Sensitive to crystal symmetry	Advantages	Disadvantages
PPN (this work)	x		10-30 nm	X	Access to vibrational fingerprint of minerals, orientation dependence	AFM tip in sample environment
tip-enhanced Raman ³⁵		X	<100 nm	X	Access to vibrational fingerprint of minerals, orientation dependence	AFM tip in sample environment, Photodamage risk, tip degradation
nano FTIR ¹²	x		few 10 nm		Access to vibrational fingerprint of minerals	AFM tip in sample environment

polarized PPN spectrum (Figure 3b). From this finding, a different crystal axis orientation compared to the olivine single crystal (Figure 2) can be concluded. A further quantitative determination of the orientation is, in principle, possible but is beyond the scope of this article. It would require detailed research of the Christiansen features in dependence on the azimuthal rotation, an optical simulation of the direction-dependent absorption properties in the range of the vibrational bands, and a quantitative understanding of the correlation between photothermal expansion and the absorption properties in dependence on the penetration depths of radiation.

The frequencies of the 3,4 peaks are chosen for further sand p-polarized imaging (Figure 3 c-f). It can be seen that the nanosized crystal grain crystallite is well separated from the surrounding olivine because of the different AFM cantilever bending mode frequencies in these two areas. The PPN signal along a selected line (yellow, dotted, Figure 3f) is presented in Figure 3g.

In summary, the results prove that phenomenological fingerprints and orientation information can be achieved on the nanoscale at sub-50-nm resolution.

Olivine Inclusions in a Glass Matrix. In Figure 4b, the sand p-polarization-dependent PPN spectra of an olivine inclusion in a glass matrix are displayed. The positions of characteristic bands (1 at 960 cm⁻¹; 2 at 980 cm⁻¹; 3 at 1033 cm⁻¹) are close to the positions observed previously for the olivine single crystal (Figure 2) and the multicrystalline sample (Figure 3). The different spectral signatures in the s- and p-polarized spectra indicate, once again, an anisotropic crystalline structure. The broad background observed can tentatively be assigned to the contribution of the glass matrix (see comparative measurements in Figure 4f).

A map of the p-polarized IR amplitude at 980 cm⁻¹ in Figure 4d (close to the maximum of band 2) correlates to some degree qualitatively with the morphology reflected by the AFM image in Figure 4a. Because changes in the sample stiffness or topography induce a shift in the resonance frequency,²¹ they can induce changes in the measured amplitude of the presented maps and be responsible for sharp features in the IR amplitude. They indicate changes of crystallinity and/or crystal orientation along what appear to be grain boundaries on a subnanometer level. To investigate possible spectral variations, a line of s-polarized PPN spectra was measured along 9 positions and is shown in Figure 4e.

Assuming a strict correlation between the spectra and structure, the normalized spectra in Figure 4e indicate a chemically homogeneous material for the measured single spots.

The results shown in Figure 4 prove that PPN measurements can clearly resolve the olivine crystallites in the synthetic glass matrix via the identification of characteristic spectral signatures of olivine. The polarization-dependent spectra prove an anisotropic nature of the crystallites; furthermore, there are

indications that a broadband background arises from the surrounding glass matrix. However, as also discussed with respect to the previous example, further detailed studies beyond the scope of this paper are required to gain more quantitative information and will be part of future work.

CONCLUSION

The applicability of PPN to achieve phenomenological fingerprint spectra and orientation information on olivine crystals and inclusions has been demonstrated. For a natural olivine single crystal, the orientation was determined by correlation to the literature optical constants. For all studied samples, features related to the Christiansen effect are also observed. These features appear at frequencies where n=1 and are, due to the direction-dependent optical constants, highly indicative of the orientation of an anisotropic crystal. The PPN images indicate, for both the multicrystalline olivine and the olivine inclusion in a glass matrix, spatial changes in the optical response on the submicron level. These finely and spatially resolved features can often not be correlated to features observed in the morphology and hence show the added value of PPN and its high potential in planetary science applications.

Combined microstructural and chemical analyses can be particularly relevant for mineral grains in optically transparent extraterrestrial matrices. So far, a few-tens of μ m-sized particles have typically been returned by space probes to solar system objects. Small inclusions in these particles are typically on the nanometer scale, both in size and in the distances between them. The individual chemical differentiation of grains in such assemblies requires mesoscale probing, which, as this study demonstrates, is enabled by PPN.

Macroscale crystal orientation can, in principle, also be accessed for most minerals with anisotropic lattice symmetries using polarization-resolved Raman microscopy; see, for example, the case of olivine. This also applies to many polymorphs. However, inherently low Raman scattering efficiencies imply highly focused beams, which can lead to overheating of micron-sized grains or inclusions trapped in matrices (up to several hundred degrees Another risk is photochemical alterations. On the contrary, PPN, operating at infrared wavelengths, avoids photochemistry altogether and merely induces heating of the irradiated areas by merely a few degrees and hence is noninvasive.

Table 1 shows a comparison of PPN with nanospectroscopic techniques that have, in the past, been employed to study mineral samples.

It should be noted that, although the PPN technique is in this work demonstrated on the example of olivine, the findings are applicable to all minerals exhibiting vibrational resonances within the spectral range accessible to the PPN setup.

Finally, an extension of the PPN spectral range toward longer and shorter wavelengths would be favorable, as this

would add to the chemical specificity of the technique, allowing access to a wider region of characteristic lattice and bending vibrational modes, as well as high-energy internal stretching vibrations. Intensive work on the availability of custom-made QCLs of suitable performance is in progress (see, e.g. ref 36).

AUTHOR INFORMATION

Corresponding Authors

- K. Hinrichs Nanoscale Solid-Liquid Interfaces, Helmholtz-Zentrum Berlin für Materialien und Energie GmbH, Berlin 12489, Germany; orcid.org/0000-0002-6580-7791; Email: karsten.hinrichs@helmholtz-berlin.de
- M. Gensch Institut für Weltraumforschung, DLR, Berlin 12489, Germany; Institut für Physik und Astronomie, Technische Universität Berlin, Berlin 10623, Germany; orcid.org/0000-0001-7755-1618; Email: michael.gensch@dlr.de

Authors

- T. Shay ASML Berlin GmbH, Berlin 12347, Germany; o orcid.org/0000-0001-7874-5991
- S.G. Pavlov Institut für Weltraumforschung, DLR, Berlin 12489, Germany
- N. Stojanovic Institut für Weltraumforschung, DLR, Berlin 12489, Germany
- I. Weber Institut für Planetologie, Universität Münster, Münster 48149, Germany
- A. Morlok Institut für Planetologie, Universität Münster, Münster 48149, Germany

Complete contact information is available at: https://pubs.acs.org/10.1021/acsearthspacechem.5c00124

Notes

The authors declare no competing financial interest.

■ ACKNOWLEDGMENTS

The authors thank Ilona Engler and Özgür Savaş for technical support. K.H. is grateful for the financial support provided by the Europäischer Fonds für regionale Entwicklung (EFRE) (1.8/13) (Application Lab for Infrared Ellipsometry). M.G. and N.S. acknowledge funding from the Deutsche Forschungsgemeinschaft (DFG, German Research Foundation) through the priority program SPP2314 INTEREST (project ITISA, project ID GE 3288 2-1; project ITISA2, project ID GE 3288 2-2).

REFERENCES

- (1) Howard, E. C. Experiments and observations on certain stony and metalline substances, which at different times are said to have fallen on earth; also on various kinds of iron. *Philos. Trans. R. Soc. London* **1802**, 92, 168.
- (2) Rubin, A. E. Mineralogy of meteorite groups. *Meteorit. Planet. Sci.* 1997, 32, 231.
- (3) Sprague, A. L.; Witterborn, F. C.; Kozlowski, R. W.; Cruikshank, D. P.; Bartholomew, M. J.; Graps, A. L. The Moon: Mid-infrared (7.5-to 11.4-μm) spectroscopy of selected regions. *Icarus* **1992**, *100*, 73–84.
- (4) Heyminck, S.; Graf, U. U.; Güsten, R.; Stutzki, J.; Hübers, H. W.; Hartogh, P. GREAT: The SOFIA high-frequency heterodyne instrument. *Astron. Astroph.* **2012**, *542*, L1.
- (5) Cesarky, C.; Salama, A.ISO science legacy a compact review of ISO major achievementsSpringer Science & Business Media2006

- (6) Pieters, C. M. Lunar Materials from the Visible to the Midinfrared. *Int. Geol. Rev.* **1998**, *40*, 981.
- (7) Meshik, A.; Mabry, J.; Hohenberg, C.; Marrocchi, Y.; Pravdivtseva, O.; Burnett, D.; Olinger, C.; Wiens, R.; Reisenfeld, D.; Allton, J.; McNamara, K.; et al. Constraints on Neon and Argon Isotopic Fractionation in Solar Wind. *Science* **2007**, *318*, 433.
- (8) Brownlee, D.; Tsou, P.; Aléon, J.; Alexander, C. M.; Araki, T.; Bajt, S.; Baratta, G. A.; Bastien, R.; Bland, P.; Bleuet, P.; et al. Comet 81P/Wild 2 under a microscope. *Science* **2006**, *314*, 1711–1716.
- (9) Normile, D. Spunky Hayabusa Heads Home With Possible Payload. *Science* **2010**, 328, 565.
- (10) Storz, J.; Reitze, M. P.; Stojic, A. N.; Kerraouch, I.; Bischoff, A.; Hiesinger, H.; John, T. Micro-FTIR reflectance spectroscopy of Ryugu, CI chondrites and volatile-rich clasts Comparing spectral features in the Mid-IR (2.5–16.5 μ m) region. *Icarus* **2024**, 420, 116189.
- (11) Bonal, L.; Brunetto, R.; Beck, P.; Dartois, E.; Dionnet, Z.; Djouadi, Z.; Duprat, J.; Füri, E.; Kakazu, Y.; Montagnac, G.; Oudayer, P.; Quirico, E.; Engrand, C. Visible-IR and Raman microspectroscopic investigation of three Itokawa particles collected by Hayabusa: Mineralogy and degree of space weathering based on nondestructive analyses. *Meteorit. Planet. Sci.* **2015**, *50*, 1562–1576.
- (12) Dominguez, G.; Mcleod, A. S.; Gainsforth, Z.; Kelly, P.; Bechtel, H. A.; Keilmann, F.; Westphal, A.; Thiemens, M.; Basov, D. N. Nanoscale infrared spectroscopy as a non-destructive probe of extraterrestrial samples. *Nat. Commun.* **2014**, *5*, 5445.
- (13) Kebukawa, Y.; Kobayashi, H.; Urayama, N.; Baden, N.; Kondo, M.; Zolensky, M. E.; Kobayashi, K. Nanoscale infrared imaging analysis of carbonaceous chondrites to understand organic-mineral interactions during aqueous alteration. *Proc. Natl. Acad. Sci. U. S. A.* **2019**, *116*, 753–758.
- (14) Phan, V. T. H.; Rebois, R.; Beck, P.; Quirico, E.; Bonal, L.; Noguchi, T. Nanoscale mineralogy and organic structure in Orgueil (CI) and EET 92042 (CR) carbonaceous chondrites studied with AFM-IR spectroscopy. *Meteorit. Planet. Sci.* **2022**, *57*, 3–21.

(15) Kebukawa, Y.; Mathurin, J.; Dartois, E.; Dazzi, A.; Deniset-

- Besseau, A.; Duprat, J.; Remusat, L.; Noguchi, T.; Miyake, A.; Igami, Y.; Paoletti, M. V.; Zolensky, M. E.; Engrand, C.; Sandt, C.; Borondics, F.; Yamashita, S.; Wakabayashi, D.; Takeichi, Y.; Takahashi, Y. Complex mixture of organic matter in a xenolithic clast from the Zag meteorite revealed by coordinated analyses using AFM-IR. NanoSIMS and STXM/XANES. Icarus 2023, 400, 115582. (16) Mathurin, J.; Bejach, L.; Dartois, E.; Engrand, C.; Dazzi, A.; Deniset-Besseau, A.; Duprat, J.; Kebukawa, Y.; Yabuta, H.; Bonal, L.; Quirico, E.; Sandt, C.; Borondics, F.; Barosch, J.; Beck, J.; Cody, G. D.; De Gregorio, B. T.; Hashiguchi, M.; Kilcoyne, D. A. L.; Komatsu, M.; Martins, Z.; Matsumoto, M.; Montagnac, G.; Mostefaoui, S.; Nittler, L. R.; Ohigashi, T.; Okumura, T.; Phan, V. T. H.; Remusat, L.; Sandford, S.; Shigenaka, M.; Stroud, R.; Suga, H.; Takahashi, Y.; Takeichi, Y.; Tamenori, Y.; Verdier-Paoletti, M.; Yamashita, S.; Nakamura, T.; Morita, T.; Kikuiri, M.; Amano, K.; Kagawa, E.; Noguchi, T.; Naraoka, H.; Okazaki, R.; Sakamoto, K.; Yurimoto, H.; Abe, M.; Kamide, K.; Miyazaki, A.; Nakato, A.; Nakazawa, S.; Nishimura, M.; Okada, T.; Saiki, T.; Tachibana, S.; Tanaka, S.; Terui, F.; Tsuda, Y.; Usui, T.; Watanabe, S.; Yada, T.; Yogata, K.; Yoshikawa, M. AFM-IR nanospectroscopy of nanoglobule-like particles in Ryugu samples returned by the Hayabusa2 mission. Astron. Astrophys. 2024, 684, A198.
- (17) Ruzicka, A. M.; Hugo, R. C. Electron backscatter diffraction (EBSD) study of seven heavily metamorphosed chondrites: Deformation systematics and variations in pre-shock temperature and post-shock annealing. *Geochim. Cosmochim. Acta* **2018**, 234, 115–147
- (18) Matsumoto, M.; Matsuno, J.; Tsuchiyama, A.; Nakamura, T.; Enokido, Y.; Kikuiri, M.; Nakato, A.; Yasutake, M.; Uesugi, K.; Takeuchi, A.; et al. Microstructural and chemical features of impact melts on Ryugu particle surfaces: Records of interplanetary dust hit on asteroid Ryugu. *Sci. Adv.* **2024**, *10*, No. eadi7203.

- (19) Zhang, Y.; Yilmaz, U.; Lukasievicz, G. V. B.; O'Faolain, L.; Lendl, B.; Ramer, G. An analytical model of label-free nanoscale chemical imaging reveals avenues toward improved spatial resolution and sensitivity. *Proc. Natl. Acad. Sci. U. S. A.* **2025**, 122, No. e2403079122.
- (20) Schwartz, J. J.; Jakob, D. S.; Centrone, A. A guide to nanoscale IR spectroscopy: Resonance enhanced transduction in contact and tapping mode AFM-IR. *Chem. Soc. Rev.* **2022**, *51*, 5248–5267.
- (21) Mathurin, J.; Deniset-Besseau, A.; Bazin, D.; Dartois, E.; Wagner, M.; Dazzi, A. Photothermal AFM-IR spectroscopy and imaging: Status, challenges, and trends. *J. Appl. Phys.* **2022**, *131*, 010901.
- (22) Lin, Y. T.; He, H.; Kaya, H.; Liu, H.; Ngo, D.; Smith, N. J.; Banerjee, J.; Borhan, A.; Kim, S. H. Photothermal Atomic Force Microscopy Coupled with Infrared Spectroscopy (AFM-IR) Analysis of High Extinction Coefficient Materials: A Case Study with Silica and Silicate Glasses. *Anal. Chem.* **2022**, *94*, 5231–5239.
- (23) Quaroni, L. Understanding and Controlling Spatial Resolution, Sensitivity, and Surface Selectivity in Resonant-Mode Photothermal-Induced Resonance Spectroscopy. *Anal. Chem.* **2020**, *92*, 3544–3554.
- (24) Hinrichs, K.; Shaykhutdinov, T. Polarization-Dependent Atomic Force Microscopy—Infrared Spectroscopy (AFMIR): Infrared Nanopolarimetric Analysis of Structure and Anisotropy of Thin Films and Surfaces. *Appl. Spectrosc.* **2018**, *72*, 817–832.
- (25) Dazzi, A.; Glotin, F.; Carminati, R. Theory of infrared nanospectroscopy by photothermal induced resonance. *J. Appl. Phys.* **2010**, *107*, 24519.
- (26) Brearley, A. J.; Jones, R. H. Chondritic meteorites. In *Planetary Materials*, Papike, J. J., Ed.; Mineralogical Society of America: Washington, DC, 1998, pp. 3–398.
- (27) Weber, I.; Böttger, U.; Pavlov, S. G.; Jessberger, E. K.; Hübers, H. W. Mineralogical and Raman spectroscopy studies of natural olivines exposed to different planetaryenvironments. *Planet. Space Sci.* **2014**, *104*, 163–172.
- (28) Lu, F.; Jin, M.; Belkin, M. A. Tip-Enhanced Infrared Nanospectroscopy Via Molecular Expansion Force Detection. *Nat. Photonics* **2014**, *8*, 307–312.
- (29) Dazzi, A.; Prazeres, R.; Glotin, F.; Ortega, J.-M. Local Infrared Microspectroscopy with Subwavelength Spatial Resolution with an Atomic Force Microscope Tip Used as a Photothermal Sensor. *Opt. Lett.* **2005**, *30*, 2388–2390.
- (30) Dazzi, A.; Prater, C. B.; Hu, Q.; Chase, D. B.; Rabolt, J. F.; Marcott, C. AFM—IR: Combining Atomic Force Microscopy and Infrared Spectroscopy for Nanoscale Chemical Characterization. *Appl. Spectrosc.* **2012**, *66*, 1365–1384.
- (31) Fabian, D.; Henning, T.; Jäger, C.; Mutschke, H.; Dorschner, J.; Wehrhan, O. Steps toward interstellar silicate mineralogy VI. Dependence of crystalline olivine IR spectra on iron content and particle shape. *Astron. Astrophys.* **2001**, *378*, 228–238.
- (32) Ishibashi, H.; Arakawa, M.; Ohi, S.; Yamamoto, J.; Miyake, A.; Kagi, H. Relationship between Raman spectral pattern and crystallographic orientation of a rock-forming mineral: A case study of Fo₈₉Fa₁₁ olivine. *J. Raman Spectrosc.* **2008**, *39*, 1653–1659.
- (33) Böttger, U.; Pavlov, S. G.; Deßmann, N.; Hanke, F.; Weber, I.; Fritz, J.; Hübers, H.-W. Laser-induced alteration of Raman spectra for micron-sized solid particles. *Planet. Space Sci.* **2017**, *138*, 25–32.
- (34) Weber, I.; Böttger, U.; Pavlov, Ś.; Hübers, H.-W.; Hiesinger, H.; Jessberger, E. K. Laser alteration on iron sulfides under various environmental conditions. *J. Raman Spectrosc.* **2017**, *48*, 1509–1517.
- (35) Borromeo, L.; Toccafondi, C.; Minde, M. W.; Zimmermann, U.; Andò, S.; Madland, M. V.; Korsnes, R. I.; Ossikovski, R. Application of Tip-Enhanced Raman Spectroscopy for the nanoscale characterization of flooded chalk. *J. Appl. Phys.* **2018**, *124*, 173101.
- (36) Hirayama, H.; Terashima, W.; Lin, T.-T.; Sasaki, M.Recent progress and future prospects of THz quantum-cascade lasers. In: *Proceedings of the SPIE, Novel In-Plane Semiconductor Lasers XIV*, **2015**, 9382, 938217.



CAS BIOFINDER DISCOVERY PLATFORM™

BRIDGE BIOLOGY AND CHEMISTRY FOR FASTER ANSWERS

Analyze target relationships, compound effects, and disease pathways

Explore the platform

